Published in IET Microwaves, Antennas & Propagation
Received on 21st March 2008
Revised on 22nd July 2008
doi: 10.1049/iet-map.2008.0104

ISSN 1751-8725

Efficient, numerically robust characterisation of a large, double-loop antenna array

L.C. Tatalopoulos[1] *A.I. Sotiropoulos*[1] *S.P. Skouris*[1]
H.T. Anastassiu[1,2]

[1]*Hellenic Air Force Academy, GR-1010 Dekelia, Greece*
[2]*Communications and Networks Design and Development Department, Hellenic Aerospace Industry, P.O. Box 23, GR-32009 Schimatari, Tanagra/Viotia, Greece*
E-mail: Anastasiou.Christos@haicorp.com

Abstract: Arrays of circular, double-loops are treated via a semi-analytical technique, on the basis of a Method of Moments formulation. A Pocklington-type integral equation for the current is derived and discretised via a suitable set of basis functions. The matrix corresponding to the pertinent linear system is found to consist of circulant blocks. The system is therefore analytically solvable, and hence, potential ill-conditioning, encountered in large geometry cases, cannot possibly introduce any numerical instabilities to the calculations. Introduction of a delta gap source as excitation facilitates very efficient computation of the current and input admittance. The algorithm exploits almost exclusively elementary functions and yields results in terms of a set of rapidly convergent series, applicable to extremely large loops. Data for such loops are presented for the first time in literature. The method is expected to lead in the future to very efficient designs of multi-loop arrays.

1 Introduction

Circular-loop antennas are applicable to various types of wireless links and therefore have been studied extensively in the literature. Loop arrays have also been proposed, and their analysis has been presented in several pioneering papers [1, 2]. In these works, the current distribution and the input admittance are computed via integral equation modelling and subsequent Fourier analysis, which is an extension of a similar technique, having been applied earlier to single loops [3, 4]. This method is elegant and theoretically exact, however, it is prone to limitations, because of difficulties in the computation related to the special functions it requires. Accurate calculations are time-consuming and inefficient, and the procedure is hence not easily applicable to electrically large configurations.

The approach of the problem in this paper is based on the Method of Moments (MoM) and the overall methodology is strongly related to [5, 6], where single-loop antennas were addressed. The pertinent integral equation for the currents is derived, in a way similar to [1], and finally discretised via step-pulse (pulse triplet) basis functions [5, 6] with point matching. To simplify calculations at this stage, a delta gap source is used as an excitation, which may feed either one of the two loops, or even both of them. The resulting linear system consists of a 2×2 block square matrix, comprising of four circulant sub-matrices of half the overall size. Such a matrix is analytically invertible as shown in [7] and therefore the discrete approximations of the current, the impedance and the admittance can be given by explicit mathematical expressions. Furthermore, almost all mathematical expressions involved invoke merely elementary functions. Extraction of numerically stable results is therefore possible, and their accuracy is validated through comparisons with reference solutions and measurements [1]. Novel data for very large arrays are finally presented for the first time in literature. This paper is an expanded version of [8], which briefly describes the highlights of the method. The algorithm is ideal for the efficient design of double-loop antenna arrays, as it is significantly less time-consuming than standard, analytical or numerical schemes, yet being immune to inaccuracies, possibly caused by calculation instabilities and/or matrix ill-conditioning. Future, analogous work

may relate to the use of magnetic frill current excitations, to avoid numerical instabilities near the feeding point [9], as well as multi-loop arrays.

2 Analytical formulation

The geometry of the problem consists of parallel, coaxial loops, with radii b_1 and b_2 and wire radii a_1 and a_2, respectively (Fig. 1). Assume that $b_1 \leq b_2$ and $a_{1,2} \ll b_{1,2}$, that is, the loop wires are supposed to fulfil the thin wire approximation. In the general case, the loops do not necessarily lie on the same plane, but are separated by a vertical distance D (along the z-axis). The co-ordinate system is defined as in Fig. 1, that is, the large loop lies in the $z = 0$ plane and the small loop in the $z = D$ plane (D may also be negative). As an excitation, a delta gap feed is invoked, located anywhere on either one, or even both of the loops. In Fig. 1, feeds are both positioned at $\phi = 0$, but this is not restrictive for the analysis, that is, the excitations may occur at any, even different points. Using a standard formulation, similar to [5], resulting from the pertinent boundary condition for the electric field, and assuming a $e^{j\omega t}$ time dependence, the integral equation for the currents $I_{1,2}(\phi)$ on the two loops can be compactly cast. Explicitly,

$$\begin{aligned} \boldsymbol{E}_i(r,\phi)\cdot\hat{\phi} = {} & j\omega\mu r_1' \int_0^{2\pi} G(\boldsymbol{r},\boldsymbol{r}_1')\cos(\phi-\phi')I_1(\phi')\,d\phi' \\ & + j\omega\mu r_2' \int_0^{2\pi} G(\boldsymbol{r},\boldsymbol{r}_2')\cos(\phi-\phi')I_2(\phi')\,d\phi' \\ & - \frac{1}{j\omega\varepsilon r}\int_0^{2\pi}\frac{\partial}{\partial\phi}G(\boldsymbol{r},\boldsymbol{r}_1')\frac{dI_1(\phi')}{d\phi'}\,d\phi' \\ & - \frac{1}{j\omega\varepsilon r}\int_0^{2\pi}\frac{\partial}{\partial\phi}G(\boldsymbol{r},\boldsymbol{r}_2')\frac{dI_2(\phi')}{d\phi'}\,d\phi' \end{aligned} \quad (1)$$

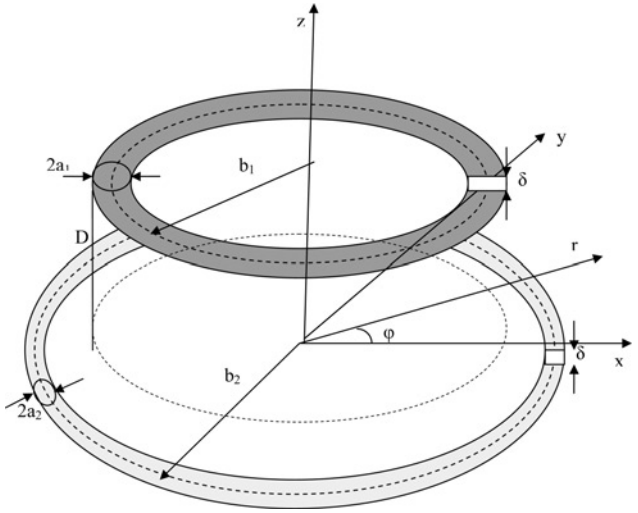

Figure 1 *Double-loop antenna array*

where G is the standard free-space scalar Green's function given by

$$G(\boldsymbol{r},\boldsymbol{r}') \equiv \frac{e^{-jk|\boldsymbol{r}-\boldsymbol{r}'|}}{4\pi|\boldsymbol{r}-\boldsymbol{r}'|} \quad (2)$$

where k is the wavenumber, μ, ε are the surrounding medium's permeability and permittivity, respectively, and $\boldsymbol{E}_i$ the incident electric field (because of the excitation). Also, $\boldsymbol{r}(r,\phi)$, $\boldsymbol{r}'(r',\phi')$ are observation and current source points, respectively and $\hat{\phi}$ is the unit vector along the azimuth direction. Index (1,2) corresponds to the loop number. Obviously, under the thin wire approximation, $r_1' = b_1$ and $r_2' = b_2$. The unknown currents $I_{1,2}(\phi')$ will be calculated from (1), after suitable discretisation and transformation to a linear system of equations, according to a standard MoM methodology. The currents on the two loops (1,2) are expanded as

$$I_{1,2}(\phi') \cong \sum_{n=1}^{N} I_n^{(1,2)} F_n(\phi') \quad (3)$$

where $F(\phi')$ are basis functions and N the number of unknowns on each loop. The key characteristic of the technique presented herein is the properties of the resulting system matrix, which will be forced to consist of circulant blocks. Owing this feature, the matrix will be inverted analytically and will thus yield the current samples in closed form. Suitable (although not unique) basis functions, facilitating this attractive property, are the step-pulses (pulse triplets) (Fig. 2) [5, 6]. Explicitly, these functions are defined as

$$F_n(\phi') \equiv \Pi_n(\phi') + \frac{1}{2}\Pi_{n-1/2}(\phi') + \frac{1}{2}\Pi_{n+1/2}(\phi') \quad (4)$$

where

$$\Pi_n(\phi') \equiv \begin{cases} 1, & \left(n-\frac{1}{4}\right)\tilde{\phi} \leq \phi' \leq \left(n+\frac{1}{4}\right)\tilde{\phi} \\ 0, & \text{else} \end{cases} \quad (5)$$

and $\tilde{\phi} \equiv 2\pi/N$.

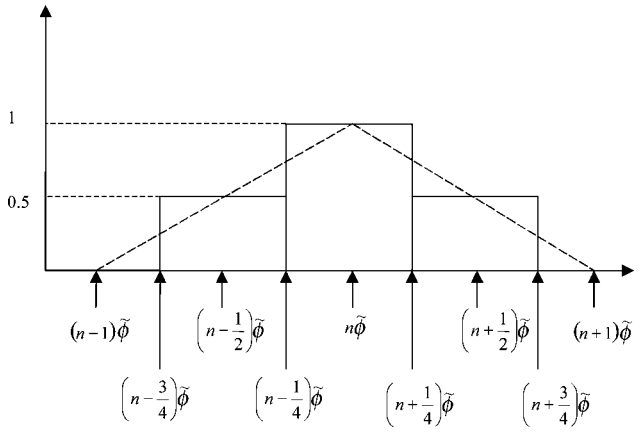

Figure 2 *Step pulse (triplet) basis functions, approximating a triangular pulse (dotted line)*

After applying point-matching at N points on each loop, that is, at $\boldsymbol{r}_{m,i} \equiv \boldsymbol{r}(r_i, \phi_m)$, where $\phi_m \equiv (m-1)\tilde{\phi}$, $m = 1, \ldots, N$ and $i = 1, 2$, then (1) yields the following system:

$$\begin{aligned} r_i \boldsymbol{E}_i(r_i, \phi_m) \cdot \hat{\phi} \cong & \mathrm{j}\omega\mu r_1' r_i \sum_{n=1}^{N} I_n^{(1)} \int_0^{2\pi} G(\boldsymbol{r}_{m,i}, \boldsymbol{r}_1') \\ & \times \cos(\phi_m - \phi') F_n(\phi') \mathrm{d}\phi' \\ & + \mathrm{j}\omega\mu r_2' r_i \sum_{n=1}^{N} I_n^{(2)} \int_0^{2\pi} G(\boldsymbol{r}_{m,i}, \boldsymbol{r}_2') \\ & \times \cos(\phi_m - \phi') F_n(\phi') \mathrm{d}\phi' \\ & - \frac{1}{\mathrm{j}\omega\varepsilon} \sum_{n=1}^{N} I_n^{(1)} \int_0^{2\pi} \frac{\partial}{\partial\phi} G(\boldsymbol{r}, \boldsymbol{r}_1') \Big|_{\boldsymbol{r}=\boldsymbol{r}_{m,i}} \frac{\mathrm{d}F_n(\phi')}{\mathrm{d}\phi'} \mathrm{d}\phi' \\ & - \frac{1}{\mathrm{j}\omega\varepsilon} \sum_{n=1}^{N} I_n^{(1)} \int_0^{2\pi} \frac{\partial}{\partial\phi} G(\boldsymbol{r}, \boldsymbol{r}_2') \Big|_{\boldsymbol{r}=\boldsymbol{r}_{m,i}} \frac{\mathrm{d}F_n(\phi')}{\mathrm{d}\phi'} \mathrm{d}\phi' \end{aligned} \tag{6}$$

After performing the integrations using the properties of pulse functions, in a way similar to [5], (6) is written in compact form as

$$[\boldsymbol{Z}]\{\boldsymbol{I}\} = \{\boldsymbol{V}\} \tag{7}$$

where

$$\{\boldsymbol{I}\} \equiv \left[I_1^{(1)} \;\; I_2^{(1)} \;\; \cdots \;\; I_N^{(1)}; \;\; I_1^{(2)} \;\; I_2^{(2)} \;\; \cdots \;\; I_N^{(2)} \right]^{\mathrm{T}} \tag{8}$$

which is the column of unknown currents,

$$\{\boldsymbol{V}\} \equiv \left[V_1^{(1)} \;\; V_2^{(1)} \;\; \cdots \;\; V_N^{(1)}; \;\; V_1^{(2)} \;\; V_2^{(2)} \;\; \cdots \;\; V_N^{(2)} \right]^{\mathrm{T}} \tag{9}$$

which is the column of excitation voltages at the matching points, related to the local incident electric field as follows:

$$V_n^{(p)} = b_p \hat{\phi} \cdot \boldsymbol{E}_i((n-1)\tilde{\phi}) \tag{10}$$

and finally $[\boldsymbol{Z}]$ is the MoM impedance matrix, conveniently split into four blocks as follows:

$$[\boldsymbol{Z}] = \begin{bmatrix} [\boldsymbol{Z}]^{(11)} & [\boldsymbol{Z}]^{(12)} \\ [\boldsymbol{Z}]^{(21)} & [\boldsymbol{Z}]^{(22)} \end{bmatrix} \tag{11}$$

The superscripts (β,γ) denote interaction between the β and the γ loop. The important feature of all four blocks is the fact that they are all circulant, for reasons explained in [5, 6]. Their entries are therefore identified by a single subscript, and after some lengthy manipulation they are finally given by

$$\begin{aligned} z_{p+1}^{(\beta\gamma)} = & \mathrm{j}k\eta b_\beta b_\gamma \Bigg[\Psi_p^{(\beta\gamma)} + \frac{\tilde{\phi}}{4} \frac{\exp\{-\mathrm{j}kR_{p+1/2}^{(\beta\gamma)}\}}{4\pi R_{p+1/2}^{(\beta\gamma)}} \\ & \times \cos\left(p + \frac{1}{2}\right)\tilde{\phi} + \frac{\tilde{\phi}}{4} \frac{\exp\{-\mathrm{j}kR_{p-1/2}^{(\beta\gamma)}\}}{4\pi R_{p-1/2}^{(\beta\gamma)}} \times \cos\left(p - \frac{1}{2}\right)\tilde{\phi} \Bigg] \\ & + \mathrm{j}\frac{\eta}{k}\frac{1}{2\tilde{\phi}} \Bigg[\frac{\exp\{-\mathrm{j}kR_{p+5/4}^{(\beta\gamma)}\}}{4\pi R_{p+5/4}^{(\beta\gamma)}} + \frac{\exp\{-\mathrm{j}kR_{p+3/4}^{(\beta\gamma)}\}}{4\pi R_{p+3/4}^{(\beta\gamma)}} \\ & - 2\frac{\exp\{-\mathrm{j}kR_{p+1/4}^{(\beta\gamma)}\}}{4\pi R_{p+1/4}^{(\beta\gamma)}} \Bigg] \\ & + \mathrm{j}\frac{\eta}{k}\frac{1}{2\tilde{\phi}} \Bigg[\frac{\exp\{-\mathrm{j}kR_{p-5/4}^{(\beta\gamma)}\}}{4\pi R_{p-5/4}^{(\beta\gamma)}} + \frac{\exp\{-\mathrm{j}kR_{p-3/4}^{(\beta\gamma)}\}}{4\pi R_{p-3/4}^{(\beta\gamma)}} \\ & - 2\frac{\exp\{-\mathrm{j}kR_{p-1/4}^{(\beta\gamma)}\}}{4\pi R_{p-1/4}^{(\beta\gamma)}} \Bigg], \quad p = 0, \ldots, N-1 \end{aligned} \tag{12}$$

where η is the medium intrinsic impedance, and

$$R_p^{(\beta\gamma)} \equiv \begin{cases} b_\beta \sqrt{4\sin^2\dfrac{p\tilde{\phi}}{2} + \left(\dfrac{a_\beta}{b_\beta}\right)^2} & \text{if } \beta = \gamma \\ \sqrt{D^2 + b_\beta^2 + b_\gamma^2 + a_\beta^2 - 2b_\beta b_\gamma \cos p\tilde{\phi}} & \text{if } \beta \neq \gamma \end{cases} \tag{13}$$

$$\begin{aligned} \Psi_p^{(\beta\gamma)} & \\ \equiv & \begin{cases} \dfrac{\tilde{\phi}}{2} \dfrac{\exp\{-\mathrm{j}kR_p^{(\beta\gamma)}\}}{4\pi R_p^{(\beta\gamma)}} \cos p\tilde{\phi}, & p \neq 0 \text{ or } \beta \neq \gamma \\ \dfrac{1}{\pi a\sqrt{1+\tau^2}} F\left(\sigma, \dfrac{\tau}{\sqrt{1+\tau^2}}\right) - \dfrac{\mathrm{j}k\tilde{\phi}}{8\pi}, & p = 0 \text{ and } \beta = \gamma \end{cases} \end{aligned} \tag{14}$$

whereas, finally [5]

$$\sigma \equiv \arcsin\left(\frac{\sqrt{1+\tau^2}\sin(\tilde{\phi}/8)}{\sqrt{1+\tau^2\sin^2(\tilde{\phi}/8)}} \right), \quad \tau \equiv \frac{2b_\beta}{a_\beta} \tag{15}$$

and

$$F(\varphi, \kappa) \equiv \int_0^{\varphi} \frac{\mathrm{d}a}{\sqrt{1-\kappa^2\sin^2 a}} \;\; \text{(elliptic integral of first kind)} \tag{16}$$

It is remarkable that in (12)–(16) mere elementary functions are employed; the only exception being the elliptic integral. Nevertheless, even the latter can be efficiently calculated via standard algorithms implemented in easily accessible library subroutines [10]. Therefore unlike standard Fourier

doi: 10.1049/iet-map.2008.0104

calculations [1], which involve several special functions of complicated nature, the entries of the impedance matrix in this paper are trivially computable. However, the most important property of the impedance matrix is its analytical invertibility, which is because of its consistence of circulant blocks. The inversion procedure is described in detail in [7], and is based on the analytical calculation of the eigenvalues of each circulant sub-matrix. A complete description of this process is found in [7] and will not be repeated here in detail. Very briefly, however, the unknown current is given as a combination of products and ratios of a set of rapidly convergent series, involving cylindrical special functions (Bessel and Hankel). The greater the number of unknowns N (appearing in the order of the cylindrical functions), the fewer terms become significant in the series, and therefore convergence is very rapid, as N increases. Convergence properties of the overall, series-based expression will be studied for specific configurations in Section 3. For an extension to matrices consisting of $M \times M$ circulant blocks, see also [11]. The most important consequence of analytical inversion is the fact that the discrete approximations of the current and the impedance/admittance are expressible by explicit formulae. Therefore very large loops become tractable, because of two reasons: (a) no numerical instabilities occur, since no numerical inversion is necessary, and hence the method is almost immune to ill-conditioning and (b) equations (12)–(16) are trivially computable, no matter how high the number of unknowns may become.

3 Numerical results

Validation of the mathematical analysis presented in Section 2 is performed via extraction of several numerical results and comparison to reference data, whenever available. The configuration, to be investigated as a first step, consists of a small loop with $kb_1 = 1$ and of a large one with $kb_2 = 1.5$. The vertical distance is originally set to $D = 0$. For both loops, we assume $b_1/a_1 = b_2/a_2 = 15$. The excitation points are always assumed to lie at $\phi = 0$. To begin with, the convergence rate of the derived series expression is examined. In all following plots, the horizontal axis corresponds to the azimuth angle along the loop circumference.

Fig. 3 depicts the convergence behaviour, as N increases, of the real part of the current $\mathrm{Re}\{I(\phi)\}$ on the small loop, when the excitation lies on the same loop. Convergence behaviour for the imaginary part is shown in Fig. 4. Similarly, Fig. 5 depicts the convergence behaviour, as N increases, of the real part of the current $\mathrm{Re}\{I(\phi)\}$ on the large loop, when the excitation lies on the small loop.

From all aforementioned plots, it is implied that, for the given radius ratio, that is, $b_1/a_1 = b_2/a_2 = 15$, convergence is achieved for a number of unknowns roughly equal to $N = 40$, that is, for an element arc length approximately equal to $\lambda/40$ for the small loop, or $\lambda/27$ for the large

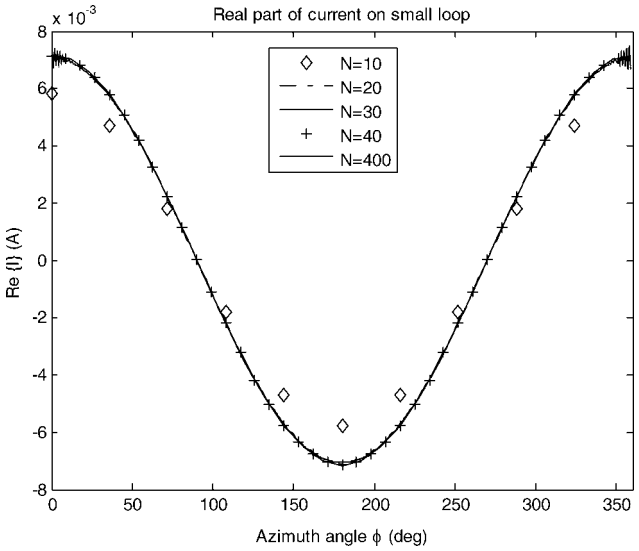

Figure 3 *Convergence of the current's real part on the small loop, when the excitation is also on the small loop*

For this configuration $kb_1 = 1$, $kb_2 = 1.5$, $D = 0$, $b_1/a_1 = b_2/a_2 = 15$

loop. It is expected that for thinner wires, convergence will be slower. Indeed, Fig. 6 depicts the convergence behaviour of a similar layout, but with $b_1/a_1 = b_2/a_2 = 150$ for the real part of the current on the small loop, when the excitation lies on the same loop. It is evident that a higher number of points are necessary; however, convergence is still achievable with reasonably coarse discretisation.

In Figs. 3–6, the solution behaviour for exceedingly large N was also depicted deliberately. As expected from analogous situations in [5, 6, 9], the use of the delta gap model yields

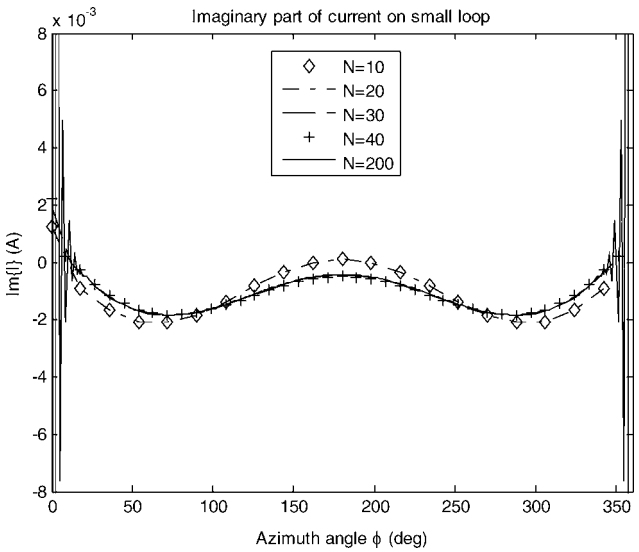

Figure 4 *Convergence of the current's imaginary part on the small loop, when the excitation is also on the small loop*

For this configuration $kb_1 = 1$, $kb_2 = 1.5$, $D = 0$, $b_1/a_1 = b_2/a_2 = 15$

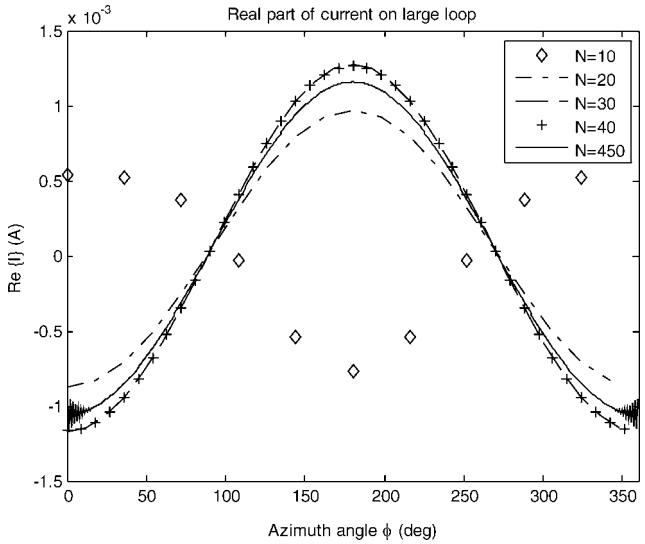

Figure 5 *Convergence of the current's real part on the large loop, when the excitation is on the small loop*

For this configuration $kb_1 = 1$, $kb_2 = 1.5$, $D = 0$, $b_1/a_1 = b_2/a_2 = 15$

unphysical oscillations of the current values close to the feeding point. In the double-loop case, this effect is discernible for both real and imaginary parts of the current, but is much more pronounced for the imaginary part, and for relatively small ratios b/a. This is the reason why calculation of the input susceptance of the double loop cannot be performed with high precision under these conditions. With increasing N, oscillations become more erratic and 'propagate' along the loop. As discussed in [9], this situation is related to the solvability of the original, pertinent integral equation for various right-hand sides (excitation models), and is not because of the algorithmic

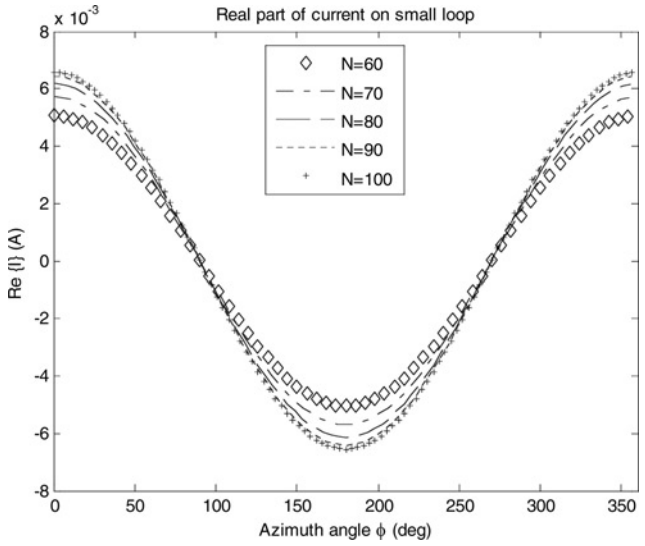

Figure 6 *Convergence of the current's real part on the small loop, when the excitation is also on the small loop*

For this configuration $kb_1 = 1$, $kb_2 = 1.5$, $D = 0$, $b_1/a_1 = b_2/a_2 = 150$

structure of the solution. It is expected that these oscillations will disappear if a magnetic frill model is invoked instead, and this issue will be investigated in some near future work.

Comparison with reference data is also possible, since pertinent measurements are found in [1] and repeated in Fig. 7 for convenience. The loops are set at different levels, separated by a vertical distance D. For this computation the wire radius is assumed to be the same in both the small and the large loops, that is, $a_1 = a_2$. The relationship between the radius of the small loop b_1 and the wire axis a_1 is given by $\Omega_1 = 2\ \ln(2\pi b_1/a_1) = 11$ or $b_1/a_1 = 38.94$. The input impedance Y_{in} is clearly the ratio of the current I to voltage V at the point where the delta source is located.

Calculations were performed for various values of kb_2, specifically for $kb_2 = 0.9$, 1.0 and 1.1 whereas kb_1 is fixed at 1.0. Results are depicted in Figs. 8 and 9, which plot the input conductance G and the input susceptance B, respectively, against the vertical distance D. The agreement of our curves with the corresponding plots in [1] is excellent. Especially, Fig. 8 is evidently identical to Fig. 7 (top) and also Fig. 9 is very similar to Fig. 7 (bottom), although not identical. Specifically, there is a small difference of about 0.5 mMho at $d/\lambda = 0.2$ at the $kb_2 = 1.0$ curve. The rather insignificant discrepancy is fully explained by the fact that the input susceptance for a delta gap model cannot be rigorously defined, since it approaches infinity as the gap width vanishes. Therefore the susceptance values calculated with a delta gap source are only good estimates of the actual ones, and become less reliable for exceedingly large N. It is mentioned that Fig. 7 also includes measured values for the input admittance, hence the accuracy of the results is guaranteed. It is expected that use of the magnetic frill current model for the excitation can improve the accuracy of the input susceptance calculations, as shown in [6] for the case of a single loop.

Far-field patterns are shown in Fig. 10, where plots are given for the $\phi = 0$ plane, as a function of θ, when $b_1/a_{1,2} = 38.94$. In Fig. 10*a* the dimensions are: $kb_1 = 1.2$, $kb_2 = 1$, $D = 0.5\lambda$, and in Fig. 10*b* the dimensions are: $kb_1 = 1.2$, $kb_2 = 1.1$, $D = 0.3\lambda$. Loop 1 is excited only at $\phi = 0$. Comparison with [1, Figure 4] shows excellent agreement.

After validating the algorithm through convergence checks and comparisons with measurements, the method will now be utilised for current computations on very large loops, for the first time in the literature. Fig. 11 shows the dependence of the input conductance as a function of the loop circumference, the latter extending to very large values. For this calculation, both loop circumferences, small and large, are increased from 1 to 40 wavelengths simultaneously, in a sense that $kb_2 = kb_1 + 1$ always. The vertical distance D between the two loops is fixed at 0 (coplanar loops). It is emphasised that the wire radius $a_{1,2}$

doi: 10.1049/iet-map.2008.0104

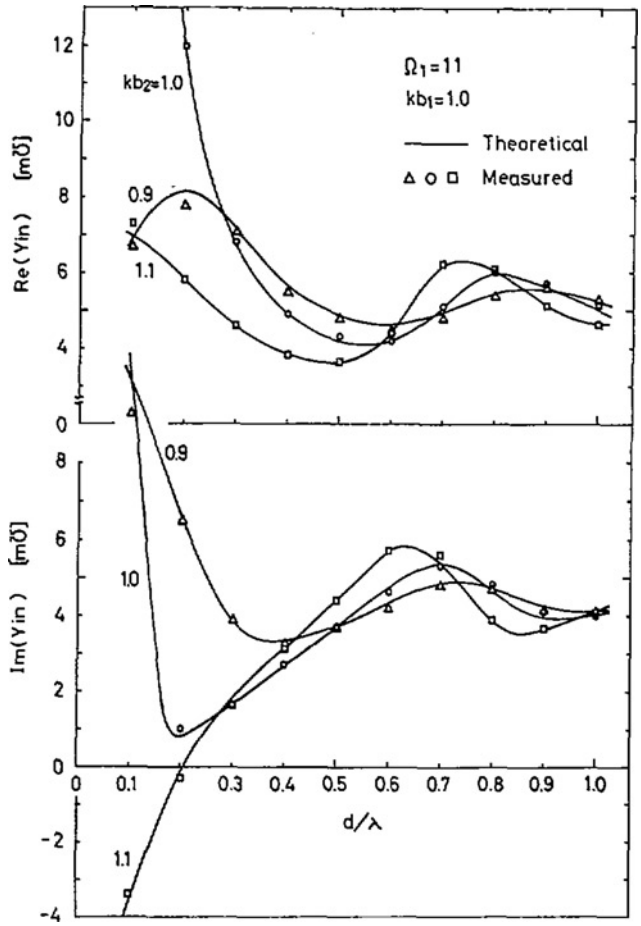

Figure 7 *Reference input conductance (above) and susceptance (bottom) as a function of the ratio D/λ for $kb_2 = 0.9, 1.0, 1.1$ and $kb_1 = 1$*

Loop 1 is driven and loop 2 is parasitic
Copied from [1, Figure 2*a*]

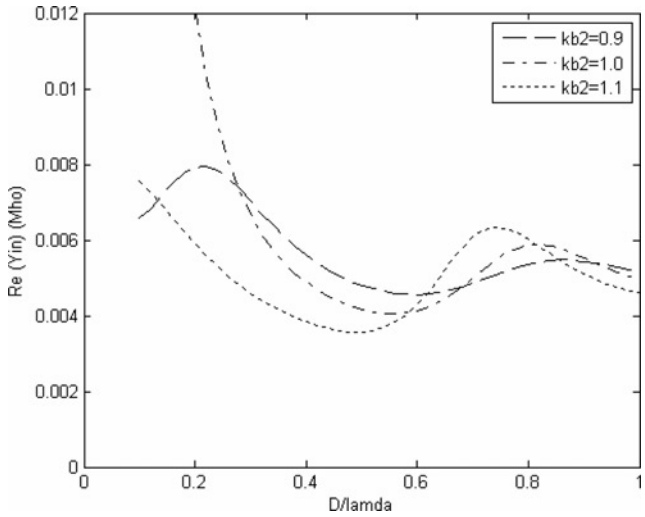

Figure 8 *Input conductance, computed by this method, as a function of the ratio D/λ for $kb_2 = 0.9, 1.0, 1.1$ and $kb_1 = 1$*

Loop 1 is driven and loop 2 is parasitic
Compare with Fig. 7

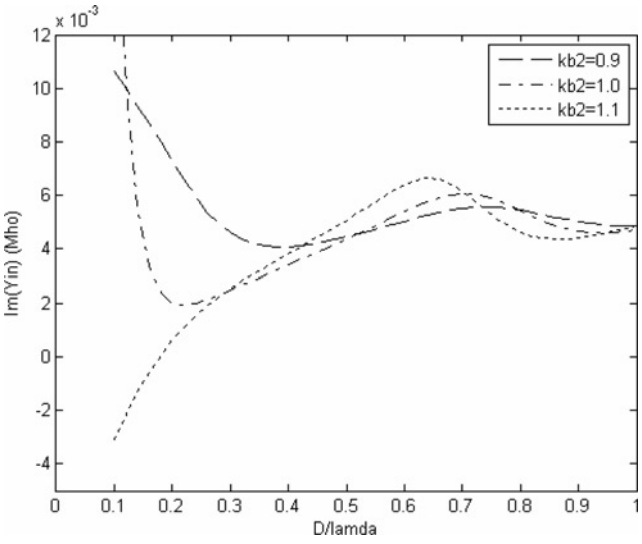

Figure 9 *Input susceptance, computed by this method, as a function of the ratio D/λ for $kb_2 = 0.9, 1.0, 1.1$ and $kb_1 = 1$*

Loop 1 is driven and loop 2 is parasitic
Compare with Fig. 7

remains constant, equal to $\lambda/100$, to meet the original assumption of the thin wire requirement. Input susceptance is not plotted for reasons explained earlier.

All calculations shown herein, including convergence checks, were performed on a typical laptop computer in a matter of a few minutes, invoking an elementary FORTRAN code. Hence, the method presented in this paper is useful for very large double-loop designs, for various reasons: it is very simple to formulate, it requires only low memory and CPU time resources, and avoids instability problems caused by possible matrix ill-conditioning, thus guaranteeing high accuracy. Finally, it may be extended in the future to multi-loop configurations, by exploiting the results in [11].

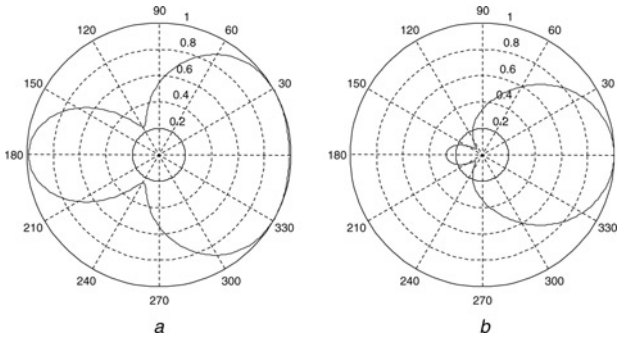

Figure 10 *Radiation field in the $\phi = 0$ plane, as a function of θ, when $b_1/a_{1,2} = 38.94$*

a $kb_1 = 1.2$, $kb_2 = 1$, $D = 0.5\lambda$
b $kb_1 = 1.2$, $kb_2 = 1.1$, $D = 0.3\lambda$
Loop 1 is excited only at $\phi = 0$
Compare with [1, Figure 4]

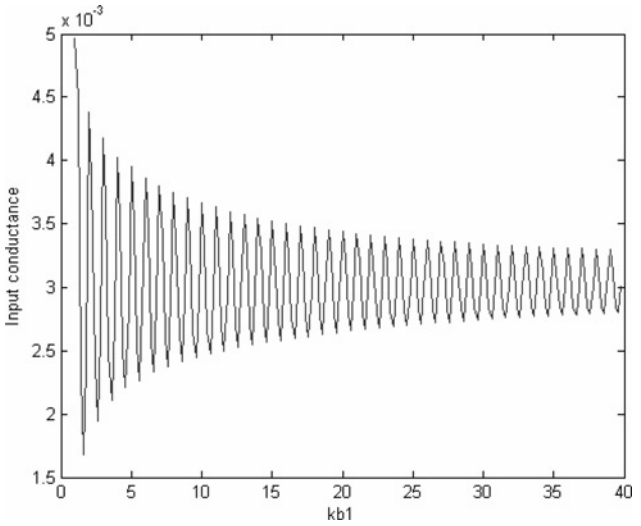

Figure 11 *Input conductance in Mho as a function of the loop circumference, extending to very large loops and* $a = \lambda/100$

For this configuration $kb_2 = kb_1 + 1$ and $D = 0$
Loop 1 is driven and loop 2 is parasitic

4 Summary and conclusions

A semi-analytical formulation was proposed for the current and far-field characterisation on a double-loop antenna array. The algorithm is particularly efficient and robust, in a sense that it is capable of yielding accurate results for loops of arbitrarily large size. The core of the algorithm was based on the MoM whose pertinent linear system was appropriately formulated in such a way that the relevant impedance matrix comprised circulant blocks. Then the system was solved analytically [7] with the help of sub-matrix diagonalisation, yielding exact expressions for the current and the input admittance. The basis functions utilised in the MoM were step pulses [5, 6]. For simplicity, a delta gap excitation was invoked in this work; however, more sophisticated feeding models should be used for reliable susceptance calculation [6]. Moreover, only elementary functions were utilised, thus facilitating easy computations for arbitrarily high numbers of unknowns. As a consequence, the results produced were numerically stable, their accuracy having been validated through comparisons with reference solutions and measurements [1]. Furthermore, completely novel data in the literature were extracted for very large loops. Finally, this work can be used in the future as a cornerstone for the efficient design of multi-loop antenna arrays, since the algorithm is much more time-efficient than standard, analytical or numerical techniques, yet retaining high accuracy, not being affected by calculation instabilities and/or matrix ill-conditioning.

5 References

[1] ITO S., INAGAKI N., SEKIGUCHI T.: 'An investigation of the array of circular-loop antennas', *IEEE Trans. Antennas Propag.*, 1971, **19**, (4), pp. 469–476

[2] SHOAMANESH A., SHAFAI L.: 'Characteristics of Yagi arrays of two concentric loops with loaded elements', *IEEE Trans. Antennas Propag.*, 1980, **28**, (6), pp. 871–874

[3] WU T.T.: 'Theory of thin circular loop antenna', *J. Math. Phys.*, 1962, **3**, pp. 1301–1304

[4] HARRINGTON R.F.: 'Field computation by moment methods' (Krieger, 1982)

[5] ANASTASSIU H.T.: 'Fast, simple and accurate computation of the currents on an arbitrarily large circular loop antenna', *IEEE Trans. Antennas Propag.*, 2006, **54**, (3), pp. 860–866

[6] ANASTASSIU H.T.: 'An efficient algorithm for the input susceptance of an arbitrarily large, circular loop antenna', *IET (IEE) Electron. Lett.*, 2006, **42**, (16), pp. 897–898

[7] ANASTASSIU H.T., KAKLAMANI D.I.: 'Error estimation and optimization of the Method of Auxiliary Sources (MAS) for scattering from a dielectric circular cylinder', *Radio Sci.*, 2004, **39**, (5), RS5015, doi: 10.1029/2004RS003028

[8] SOTIROPOULOS A.I., TATALOPOULOS L.C., ANASTASSIU H.T.: 'Efficient, semi-analytical characterization of a double-loop antenna array'. Proc. EuCAP 2007, second European Conf. on Antennas and Propagation, Edinburgh, UK, 11–16 November 2007

[9] FIKIORIS G., PAPAKANELLOS P.J., ANASTASSIU H.T.: 'On the use of nonsingular kernels in certain integral equations for thin-wire circular-loop antennas', *IEEE Trans. Antennas Propag.*, 2008, **56**, (1), pp. 151–157

[10] PRESS W.H., TEUKOLSKY S.A., VETTERLING W.T., FLANNERY B.P.: 'Numerical recipes in FORTRAN' (Cambridge, 1992, 2nd edn.)

[11] TSITSAS N.L., ALIVIZATOS E.G., KALOGEROPOULOS G.H.: 'A recursive algorithm for the inversion of matrices with circulant blocks', *Appl. Math. Comput.*, 2007, **188**, pp. 877–894

doi: 10.1049/iet-map.2008.0104